







ARTICLE

Application of physiologically-based pharmacokinetic model approach to predict pharmacokinetics and drug–drug interaction of rivaroxaban: A case study of rivaroxaban and carbamazepine

Lien Thi Ngo¹  | Sung-yoon Yang¹ | Sooyoung Shin²  | Duc Tuan Cao³  |
Hung Van Nguyen⁴  | Sangkeun Jung⁵ | Jae-Young Lee⁵ | Jong-Hwa Lee^{6,7} |
Hwi-yeol Yun¹  | Jung-woo Chae¹ 

¹College of Pharmacy, Chungnam National University, Daejeon, Korea

²College of Pharmacy, Ajou University, Suwon, Korea

³Department of Pharmaceutical Chemistry and Quality Control, Faculty of Pharmacy, Haiphong University Medicine and Pharmacy, Haiphong, Vietnam

⁴Department of Pharmacology, Faculty of Pharmacy, Haiphong University Medicine and Pharmacy, Haiphong, Vietnam

⁵Department of Computer Science and Engineering, Chungnam National University, Daejeon, Korea

⁶Korea Institute of Toxicology, Daejeon, Korea

⁷Department of Human and Environment Toxicology, University of Science and Technology, Daejeon, Korea

Correspondence

Jung-woo Chae and Hwi-yeol Yun,
College of Pharmacy, Chungnam
National University, Daejeon 34134,
Korea.

Email: jwchae@cnu.ac.kr, hyyun@cnu.ac.kr

Jong-Hwa Lee, Korea Institute of
Toxicology, 34114 Daejeon, Korea.
Email: jhl@kitox.re.kr

Funding information

Korea Ministry of Environment (MOE);
Environmental Diseases Prevention and
Management, Grant/Award Number:
2021003310001; Korea Environmental
Industry & Technology Institute
(KEITI); National Research Foundation
of Korea (NRF), Grant/Award
Number: NRF-2022R1A2C1010929
and NRF-2018R1C1B5085278; Korean

Abstract

Rivaroxaban (RIV; Xarelto; Janssen Pharmaceuticals, Beerse, Belgium) is one of the direct oral anticoagulants. The drug is a strong substrate of cytochrome P450 (CYP) enzymes and efflux transporters. This study aimed to develop a physiologically-based pharmacokinetic (PBPK) model for RIV. It contained three hepatic metabolizing enzyme reactions (CYP3A4, CYP2J2, and CYP-independent) and two active transporter-mediated transfers (P-gp and BCRP transporters). To illustrate the performance of the developed RIV PBPK model on the prediction of drug–drug interactions (DDIs), carbamazepine (CBZ) was selected as a case study due to the high DDI potential. Our study results showed that CBZ significantly reduces the exposure of RIV. The area under the concentration–time curve from zero to infinity (AUC_{inf}) of RIV was reduced by 35.2% (from 2221.3 to 1438.7 ng*h/ml) and by 25.5% (from 2467.3 to 1838.4 ng*h/ml) after the first dose and at the steady-state, respectively, whereas the maximum plasma concentration (C_{max}) of RIV was reduced by 37.7% (from 266.3 to 166.1 ng/ml) and

Lien Thi Ngo, Sung-yoon Yang and Sooyoung Shin contributed equally to this work as the first-authors.

Jong-Hwa Lee, Hwi-yeol Yun and Jung-woo Chae contributed equally to this work as the corresponding authors.

This is an open access article under the terms of the [Creative Commons Attribution-NonCommercial](https://creativecommons.org/licenses/by-nc/4.0/) License, which permits use, distribution and reproduction in any medium, provided the original work is properly cited and is not used for commercial purposes.

© 2022 The Authors. *CPT: Pharmacometrics & Systems Pharmacology* published by Wiley Periodicals LLC on behalf of American Society for Clinical Pharmacology and Therapeutics.

Government (MSIT), Grant/Award
Number: 2020-0-01441 and RS-
2022-00155857

36.4% (from 282.3 to 179.5 ng/ml), respectively. The developed PBPK model of RIV could be paired with PBPK models of other interested perpetrators to predict DDI profiles. Further studies investigating the extent of DDI between CBZ and RIV should be conducted in humans to gain a full understanding of their safety and effects.

Study Highlights

WHAT IS THE CURRENT KNOWLEDGE ON THE TOPIC?

A physiologically-based pharmacokinetic (PBPK) model of rivaroxaban (RIV) has been previously developed and applied for the prediction of drug-drug interactions (DDIs) for RIV. However, the efflux function of P-gp/BCRP transporters is not implemented in the model.

WHAT QUESTION DID THIS STUDY ADDRESS?

A PBPK model for RIV to improve the previously published model was developed. In this model, in addition to the hepatic enzymatic (CYP3A4, CYP2J2, and non-CYP) reactions, the P-gp/BCRP transporter-mediated transfer was implemented. A case study of carbamazepine (CBZ) was selected to illustrate the performance of the developed model on the prediction of DDI profiles of RIV.

WHAT DOES THIS STUDY ADD TO OUR KNOWLEDGE?

A PBPK model of RIV that described well both the plasma concentration-time profiles, the eliminations profiles in urines and feces, and the hepatic metabolism profiles of RIV, was developed. This model was applied to predict the DDIs between CBZ and RIV. Further evaluation is needed to refine the P-gp/BCRP efflux transport parameterizing.

HOW MIGHT THIS CHANGE DRUG DISCOVERY, DEVELOPMENT, AND/OR THERAPEUTICS?

The developed PBPK of RIV could be applied for the prediction of DDIs between RIV and other interested enzymes/transporters perpetrators.

INTRODUCTION

Rivaroxaban (RIV; Xarelto; Janssen Pharmaceuticals, Beerse, Belgium) is one of the direct oral anticoagulants (DOACs) that binds directly and reversibly to the active site of factor Xa (both free and thrombin-bound forms). By completely inhibiting factor Xa activity and prothrombinase activity, RIV decreases thrombin generation. RIV has been approved for clinical use to prevent and treat venous and arterial thromboembolic events in many countries.

Both the liver and kidneys eliminate RIV. About 43% of the administered dose is eliminated as the unchanged drug compound, including 36% eliminated in the urine (6% is excreted via glomerular filtration and 30% via active renal transportation) and about 7% eliminated in the feces. About 46% of the administered dose is subject to metabolic degradation. Cytochrome P450 (CYP) 3A4/A5 accounts for about 18% of the total RIV dose, CYP2J2 accounts for about 14%, and CYP-independent hydrolysis mechanism (non-CYP-mediated hydrolysis of the amide bonds) accounts for ~14% of the administered dose. About

11% of the administered dose (the remaining dose) is unaccounted for RIV elimination.¹⁻³

P-glycoprotein (P-gp) or multi-drug resistance protein 1 (MDR1, ABCB1) and breast cancer resistance protein (BCRP) transporters belong to the ATP-binding cassette family of efflux transporters. Both are expressed in various organs, primarily in the liver, kidneys, and gastrointestinal tract. They contribute to their substrate drugs' absorption and elimination process. In vitro and in vivo drug interaction studies of RIV suggest that P-gp and BCRP transporters are involved in the active transportation of the drug.⁴⁻⁷ They were assumed to account for the renal active elimination of 30% of the administered dose. In vivo, the absence of both P-gp and BCRP transporters synergistically and significantly alters RIV disposition.⁷ In addition, there is a 2.5-fold increase in the area under the plasma concentration-time curve (AUC) of RIV when RIV is concomitantly administered with ketoconazole (a strong inhibitor of both CYP3A4 and P-gp/BCRP) or ritonavir (a strong inhibitor of CYP3A4 and weak inhibitor of P-gp/BCRP).⁴

Considering the therapeutic indications, RIV is likely to be administered in combination with various drugs.

As being a strong substrate of the metabolic enzymes (CYP3A4/A5, CYP2J2, and non-CYP hydrolysis enzymes) and transporters (P-gp and BCRP), drug–drug interactions (DDIs), one of the most common causes of adverse drug reactions, could be expected when RIV is concomitantly administered with these enzyme and transporter perpetrators. Investigation of the potential DDI is imperative.

A physiologically-based pharmacokinetic (PBPK) model for RIV was developed in adults and scaled to the pediatric population by Willmann et al.⁸ The model was applied for several purposes, including the prediction of the potential DDI of RIV.^{9–11} The role of active transporters (P-gp/BCRP) was not directly implemented in that model. For application purposes relevant to transporters, the efflux function of the P-gp was considered in the renal elimination process. The authors assumed that P-gp was the major transport protein accounting for the net tubular secretion of RIV. For example, to scale the developed PBPK model of RIV in adults to children, the authors indirectly calculated the age-dependence of net tubular secretion through the age-dependency profile of P-gp (using digoxin as a marker of the P-gp transporter in the human kidneys).⁸ By accounting for at least the elimination of 30% of the administered dose (in the renal), the role of transporters (P-gp/BCRP) is significant. Of note, in addition to the kidneys, it is well known that P-gp/BCRP is primarily expressed at the apical membrane of the gastrointestinal tract and liver. They contribute to the portion of RIV that pass through the gut (drugs will be eliminated into feces if they did not pass through the gut) and are metabolized in the liver. However, the efflux transport function of P-gp in all other organs, except the renal, was not considered in the RIV PBPK model of Willmann et al.⁸ We aimed to develop a PBPK model for RIV that improves the previously developed model of Willmann et al.⁸ The efflux activity of P-gp and also BCRP in all expressed locations were included. Considering that RIV follows a dose-dependent PK profile,¹² all of the latest RIV PK profiles with a broad dose range (from 1.25 to 80mg) were collected in both fasted and fed conditions. After that, the PBPK model for RIV developed in this study was further applied to predict the RIV DDI potential. Herein, we describe a case study using carbamazepine (CBZ), one of the recommended first-line options for the treatment of seizures and epilepsy, to illustrate the performance of PK-Sim (Open Systems Pharmacology Suite 9.1, licensed by the Open Systems Pharmacology community, www.open-systems-pharmacology.org) in predicting the DDI profile between RIV and CBZ. CBZ is well-known as a strong inducer of CYP enzymes^{13,14} and P-gp transporters.^{15,16} The drug decreases the exposures of CYP3A4 and P-gp substrate medications when they are co-administered.^{16–19} CBZ interacts with ivabradine, a strong substrate of CYP3A4, in healthy volunteers, and lowers its

bioavailability by about 80%.¹⁹ CBZ significantly alters the pharmacokinetics (PKs) of fexofenadine, a strong substrate of P-gp. A decrease of about 40% in the AUC is observed.¹⁸ As RIV is a strong substrate of CYP3A4 and P-gp, DDIs between RIV and CBZ could be expected.

METHODS

The PBPK model of RIV was developed and all the models were performed using PK-Sim software. Clinical PK data used for model development (training datasets) and evaluation (test datasets) were extracted from previous publications using the WebPlotDigitizer tool (<https://automeris.io/WebPlotDigitizer/>).²⁰

For the development and evaluation, the PBPK model of RIV was performed in virtual individuals. Individual demographics (i.e., race, sex, age, weight, and body mass index) were generated based on those noted in each clinical study. If there was no demographic information, one default individual (30 years of age, male, European, and a default mean weight and height according to the PK-Sim population databases) was created. Physiological parameters were provided within the software. Whenever available, the PK-Sim expression database reverse transcription-polymerase chain reaction (RT-PCR) profiles were used to define the relative tissue expression of enzymes and transporters. Drug-dependent parameters (i.e., physicochemical and absorption, distribution, metabolism, and excretion [ADME] properties) and formulation-dependent parameters (dissolution profile) were extracted from the literature.

The PBPK model of RIV was built containing three hepatic metabolizing enzyme reactions and two active transporter-mediated transfers. The hepatic metabolism of RIV included the metabolism by CYP3A4, CYP2J2, and CYP-independent hydrolysis.^{1,21,22} P-gp and BCRP were the two transporters accounting for the active transfer of RIV.^{4–7} As they are primarily expressed at the apical membrane of the gastrointestinal tract, the liver, and the kidneys' proximal tubules, these transporters contribute to the transfer of RIV across the gut, in the hepatic metabolism, and the renal active elimination. The passive renal elimination of RIV through the glomerular filtration was also included. The glomerular filtration fraction was fixed to one. The hepatic metabolism and the active transfer of RIV were assumed to follow the Michaelis–Menten type kinetics, as described in the below equation:

$$v = \frac{[E] * K_{cat} * [S]}{K_m + [S]} \quad (1)$$

where $[E]$ is the enzyme/transporter concentration, K_{cat} is the catalytic/transport rate constant, $[S]$ is the substrate concentration, and K_m is the Michaelis–Menten constant.

The workflow of the model development and evaluation for RIV is presented in Figure 1. A summary of clinical datasets and parameters used in the PBPK model are listed in Tables 1 and S1 (Supplementary Material S1). In summary, the model was initially developed based on three clinical plasma concentration-time profiles,^{12,21} one fecal elimination profile,¹² one urinary elimination profile,¹² and three hepatic

metabolism profiles (metabolism by CYP3A4, CYP2J2, and non-CYP hydrolysis metabolism).¹² All these data were observed following the administration of RIV in the solution form.

K_m and K_{cat} parameters were used to model the enzymatic reactions. For the CYP3A4 and CYP2J2 reactions, K_m values were taken from the literature³⁰; they were 46.98 and 19.37 μM , respectively. For

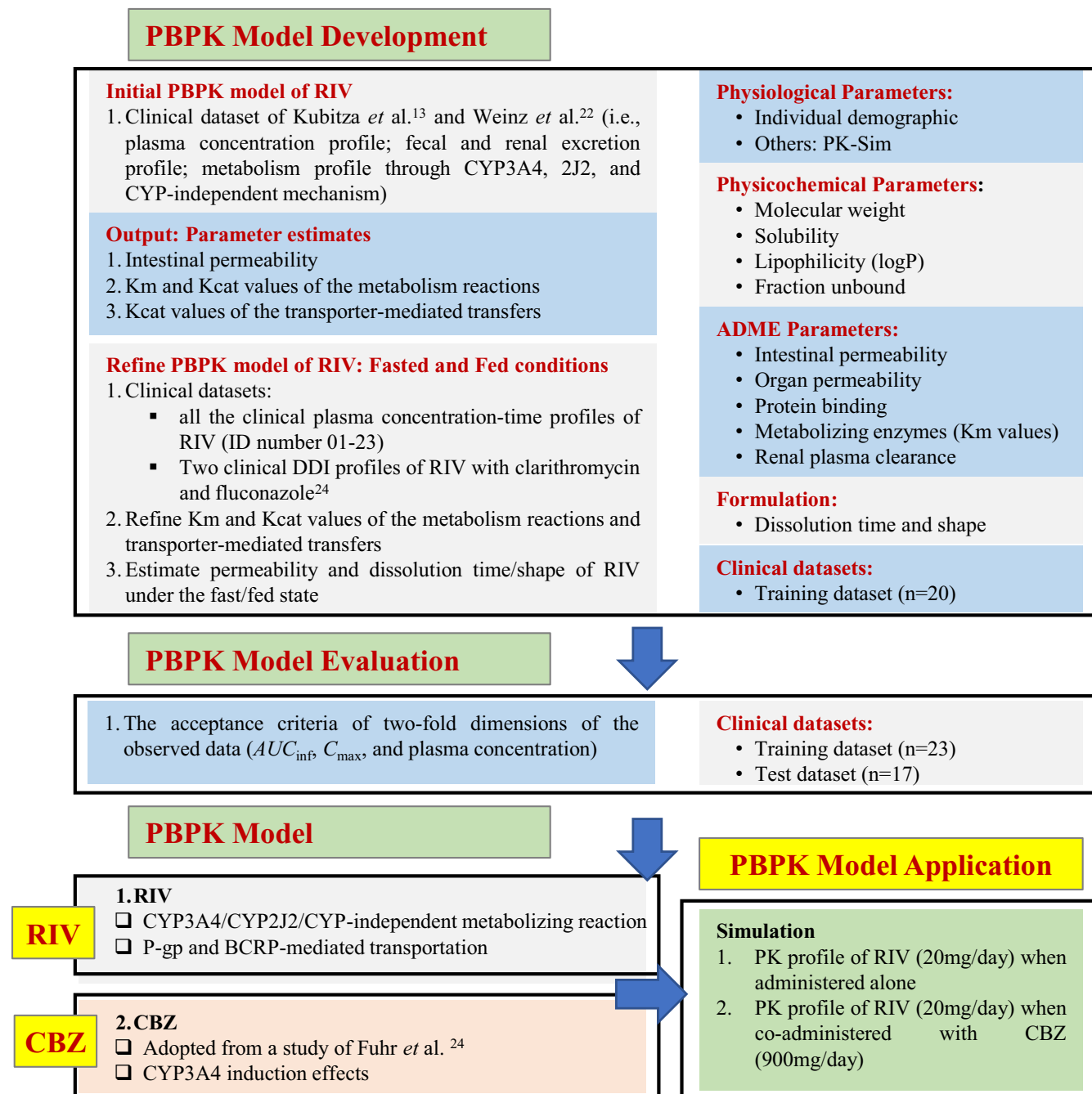


FIGURE 1 The workflow of the PBPK model development and evaluation for RIV and its application to predict drug–drug interaction between RIV and CBZ in humans. AUC_{inf} , area under the concentration-time curve from zero to infinity; CBZ, carbamazepine; C_{max} , maximum plasma concentration; K_{cat} , catalytic/transport rate constant; K_m , Michaelis–Menten constant; PBPK, physiologically-based pharmacokinetic; PK, pharmacokinetic; RIV, rivaroxaban.

TABLE 1 Input parameters and optimized parameters for the PBPK model of RIV

Parameter	Value	Unit	Literature	Note
Physicochemical properties				
MW ²³	435.88	g/mol	435.88	
Lipophilicity (LogP) ^{24,25}	0.57	–	0.57/1.36/1.5/1.74/2.18	
Fraction unbound in plasma ^{1,24,26,27}	6.74	%	2–13	Optimized
Solubility ^{24,25,28,29}	Solution: 9.9 (supersaturation) Tablet: 9.9 (fasted state) 16.8 (fed state)	mg/L	Unbuffered water (pH 7.0): 5–7/10.4/25.05 FaSSIF (pH 6.5): 9.9 FaSSGF (pH 1.6): 11.0 FeSSIF (pH 5.0): 16.8 FeSSGF (pH 4.5): 24.0	
ADME parameters				
Absorption				
Specific intestinal permeability ²⁸	2.24E-7 (fasted state, solution) 2.66E-7 (fasted state, tablet) 3.44E-7 (fed state, tablet)	cm/s	2.69E-6/8E-6	Optimized
Distribution				
Partition coefficients	PK-Sim Standards			
Cellular permeabilities	PK-Sim Standards			
Specific organ permeability	5.84E-8	cm/s	–	Optimized
Specific binding with factor Xa, K _d and K _{off}	0.005 1/s; 0.29 nM		0.005 1/s; 0.29 nM	
Metabolism				
CYP3A4_ K _m ³⁰	46.98	μM	46.98	
CYP3A4_ K _{cat}	9.77	1/min	–	Optimized
CYP2J2_ K _m ³⁰	19.37	μM	19.37	
CYP2J2_ K _{cat}	4.67	1/min	–	Optimized
CES1_ K _m	46.98	μM	–	Assumption
CES1_ K _{cat}	56.12	1/min	–	Optimized
Transport and excretion				
P-gp K _{cat}	1.25	1/min	–	Optimized
BCRP K _{cat}	0.25	1/min	–	Optimized
Dissolution profile:				
Dissolution time/shape ²⁸	0.90 h/1.27 (fasted state) 4.27 h/1.120 (fed state)		2.48 h/1.121 (fasted state) 1.47 h/1.125 (fed state)	

Abbreviations: ADME, absorption, distribution, metabolism, and excretion; BCRP, Breast cancer resistance protein; FaSSIF, fasted state simulated intestinal fluid; FaSSGF, fasted state simulated gastric fluid; FeSSIF, fed state simulated intestinal fluid; FeSSGF, fed state simulated gastric fluid; RIV, rivaroxaban.

non-CYP-mediated reaction, human carboxylesterase 1 (CES1), located in the liver and responsible for the hydrolysis of ester and amide bonds of many drugs, was introduced into the model of RIV as a representative. The K_m value for the reaction was assumed as the same as the value of the CYP3A4 reaction (i.e., 46.98 μM). The K_{cat} values for all reactions were estimated by parameter identification steps. For transporter-mediated transfer, the transporter concentration and K_m values were fixed at the default value within the PK-Sim (fixed to 1 μM). The K_{cat} values were estimated by parameter identification steps. The model structure parameters

were then refined by fitting the model to clinical plasma concentration-time profiles of the training datasets.

To inform the optimization of metabolic and transportation kinetics, the DDI between RIV and clarithromycin (a strong CYP3A4 and weak P-gp inhibitor) and the DDI between RIV and fluconazole (a moderate CYP3A4 inhibitor) were added to the training dataset.⁴ PBPK models of clarithromycin and fluconazole performing using PK-Sim, which is available on the “[Github.com](https://github.com)” library, were picked up.

The performance of a PBPK model during the model development and evaluation was assessed by comparing

the predicted and observed values of (1) the plasma concentration-time profiles and (2) the PK parameters (AUC_{inf} [AUC from zero to infinity], and C_{max}) of the drug. For quantitative measurement, the mean relative deviation (MRD) of the predicted plasma concentrations and the geometric mean fold error (GMFE) of the predicted PK parameters were calculated. The MRD and GMFE were calculated as described in the equations below:

$$MRD = 10^x, \text{ with } x = \sqrt{\frac{1}{m} \sum_{i=1}^m (\log_{10} C_{pred,i} - \log_{10} C_{obs,i})^2} \quad (2)$$

$$GMFE = 10^x, \text{ with } x = \frac{1}{n} \sum_{i=1}^n |(\log_{10} PK_{pred,i} - \log_{10} PK_{obs,i})| \quad (3)$$

where $C_{pred,i}$ is the predicted plasma concentration, $C_{obs,i}$ is the corresponding observed plasma concentration, and m is the number of observed concentrations. $PK_{pred,i}$ is the predicted AUC_{inf} or C_{max} value, $PK_{obs,i}$ is the observed AUC_{inf} or C_{max} value, and n is the number of studies. The prespecified acceptance criterion during the model development and evaluation was that the predicted parameters were within the two-fold dimension of the observed data. In addition, for visualization, the comparisons between predicted and observed plasma concentrations and PK parameters in goodness-of-fit (GOF) plots were also presented.

After the evaluation of the RIV PBPK model, an integrated PBPK model of RIV and CBZ was performed to simulate the PK profile of RIV in the absence and presence of CBZ co-administration. In this step, the simulation was carried out in a Japanese population with a virtual population ($n = 100$, 50% women) with an age range of 20–50 years and without specific body weight or height restrictions as implemented in PK-Sim.

A PBPK model of CBZ, adopted from a study by Fuhr et al.,³¹ was applied to predict the DDI between RIV and CBZ in this study. Although the induction effect of CBZ on P-gp transporter is well known,^{15–19} due to a lack of studies parametrizing this effect, the P-gp transport was not implemented in the available developed PBPK CBZ model. The CBZ-mediated CYP3A4 induction effect was described using a maximum effect (E_{max}) model, as described in the equations below:

$$\frac{dE(t)}{dt} = R_{syn,ind} - K_{deg} \times E(t) \quad (4)$$

$$R_{syn,ind} = R_{syn} \times \left(1 + \frac{E_{max} \times [Ind]}{EC_{50} + [Ind]} \right) \quad (5)$$

where $E(t)$ is the enzyme concentration; R_{syn} and $R_{syn,ind}$ are the synthesis rates of the enzyme in the absence and presence of the inducer CBZ, respectively; K_{deg} is the degradation rate constant; E_{max} is the maximal induction effect brought on by CBZ; EC_{50} is the concentration of CBZ that gives a half-maximal induction effect; and $[Ind]$ is the free CBZ concentration.

DDIs between CBZ and RIV in healthy subjects were evaluated by comparing the PK profiles of RIV in the control and test groups. For the test group, subjects received 900 mg/day of CBZ (450 mg, twice/daily) for 6 consecutive days (days 1–6). During days 7 to 12, subjects additionally received RIV doses (20 mg, once/daily) in the morning concomitantly with CBZ doses (450 mg, twice/daily). In the control group, subjects received RIV doses only (20 mg once daily) for 6 consecutive days (days 7–12) without any CBZ doses (days 1–12).

The sensitivity of the final models was assessed to measure which input parameters impact the output curves most. Parameters were included in the analysis if they were optimized, if they were associated with optimized parameters, or if they might have significant variations due to calculation methods. Accordingly, K_m and K_{cat} values for enzymatic reactions, specific intestinal permeability, dissolution time and shape, solubility, lipophilicity, factor Xa binding kinetics, and fraction unbound were included in the analysis.

RESULTS

Development and evaluation of the PBPK model of RIV

The whole-body PBPK models of RIV were developed and evaluated using a total of 40 clinical studies (Table S1, Supplementary Material S1). The PBPK models for RIV in the fed state and fasted state were developed separately.

Initially, the model was developed based on three clinical plasma concentration-time profiles, one fecal elimination profile, one urinary elimination profile, and three hepatic metabolism profiles (metabolism by CYP3A4, CYP2J2, and non-CYP hydrolysis metabolism). All these data were observed following the administration of RIV in the solution form.^{12,21} It is known that RIV is metabolized via CYP3A4/3A5 (which accounts for about 18% of total RIV dose), CYP2J2 (accounts for about 14%), and CYP-independent mechanism (non-CYP-mediated hydrolysis of the amide bonds, accounts for about 14%).^{1–3} Furthermore, it is known that about 36% and 7% of the administered dose, respectively, are excreted in the renal and feces as an unchanged compound.³ Therefore, based on the time-dependent cumulative excretion profile of

RIV reported by Weinz et al.,²¹ the time-dependent excretion profile of RIV in the renal and feces, as well as the time-dependent metabolism profiles of RIV (via CYP4A4, 2J2, and non-CYP reactions), were drawn. These profiles together with three clinical plasma concentration-time profiles were used for the initial model development. The model parameters were then refined by fitting the model to clinical plasma concentration-time profiles of all the training datasets.

The final model parameters for the PBPK model of RIV are listed in Table 1. As seen, the solubilities of RIV under the fasted and fed conditions were 9.9 and 16.8 mg/L, respectively. The specific intestinal permeability of RIV was 2.24×10^{-7} cm/s when the drug was administered as an RIV solution under the fast state, and 2.66×10^{-7} and 3.44×10^{-7} cm/s when it was administered as a tablet under the fast and fed state, respectively. The dissolution time (the time at which 50% of the dose releases from the table form) was 54 and

256 min, respectively. The K_{cat} values for the CYP3A4, 2J2, and CYP-independent reactions were 9.77, 4.67, and 56.12 1/min, respectively. The K_{cat} values for the P-gp and BCRP mediated transfer were 1.25 and 0.28 1/min, respectively. The organ permeability of RIV was 5.84×10^{-8} cm/s.

Results of the evaluation steps for the developed models are presented in Figures 2–4, Table S2, and Figure S1 (Supplementary Material S1) showing that the developed model described well the PK profiles of RIV in a wide dose range (from 1.25 to 80 mg), not only the plasma concentration-time profile but also the elimination profiles in urine and feces. The hepatic metabolism profiles and the DDI profiles of RIV with two CYP3A4/P-gp perpetrators were also well predicted (Figure S1). Only one PK parameter value (over 104 values of AUC_{inf} and C_{max} parameters) was out of the twofold acceptance range. The GMFE values for the PK parameters are 1.229 and 1.263, respectively, and 73.8%

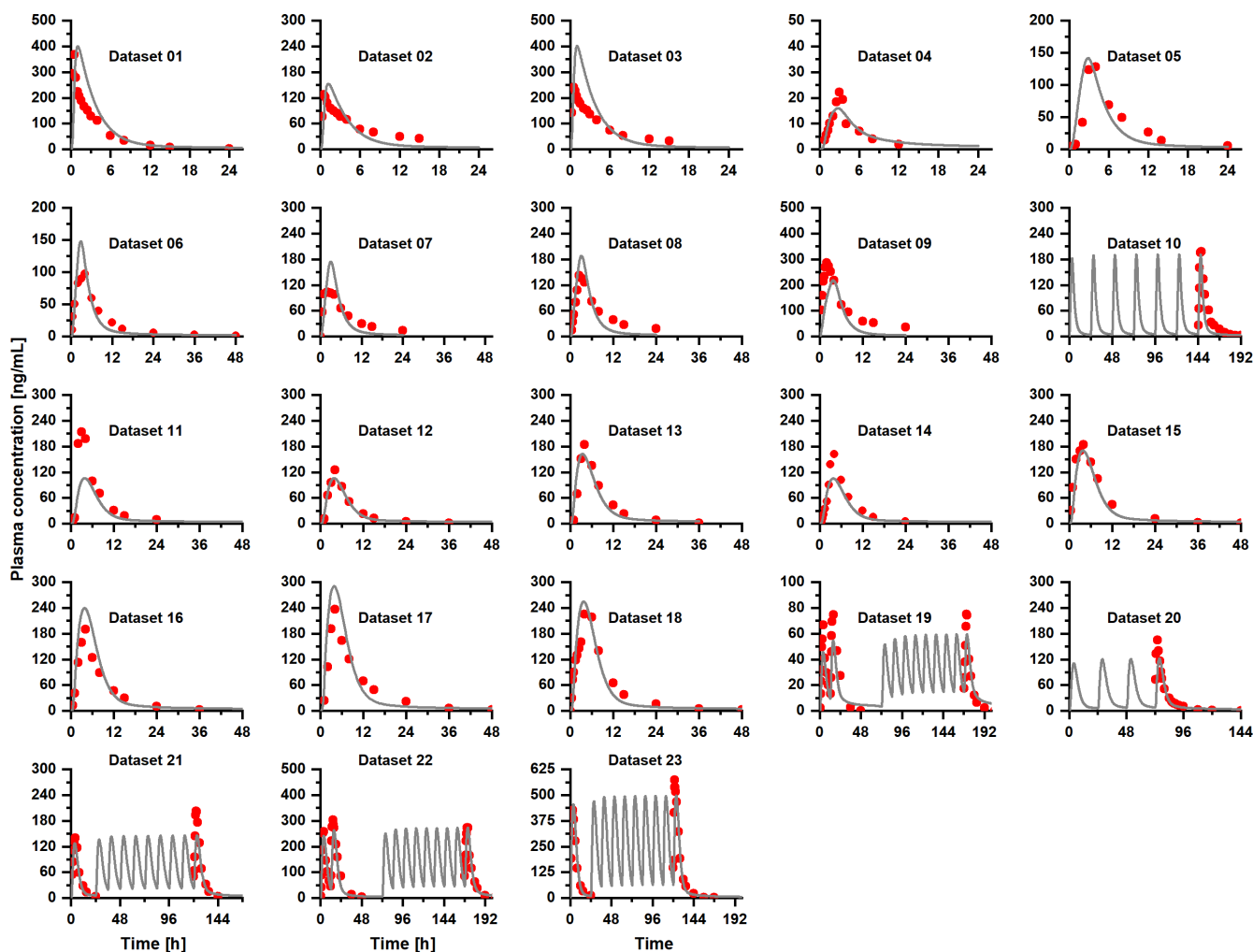


FIGURE 2 Predicted and observed plasma concentration–time curves of RIV after oral administration of RIV in healthy subjects. Training dataset. Solid lines are predicted values of each model. Circles are clinical observations. Details on dosing regimens, characteristics, subject demographics, and references are listed in Table S1. RIV, rivaroxaban.

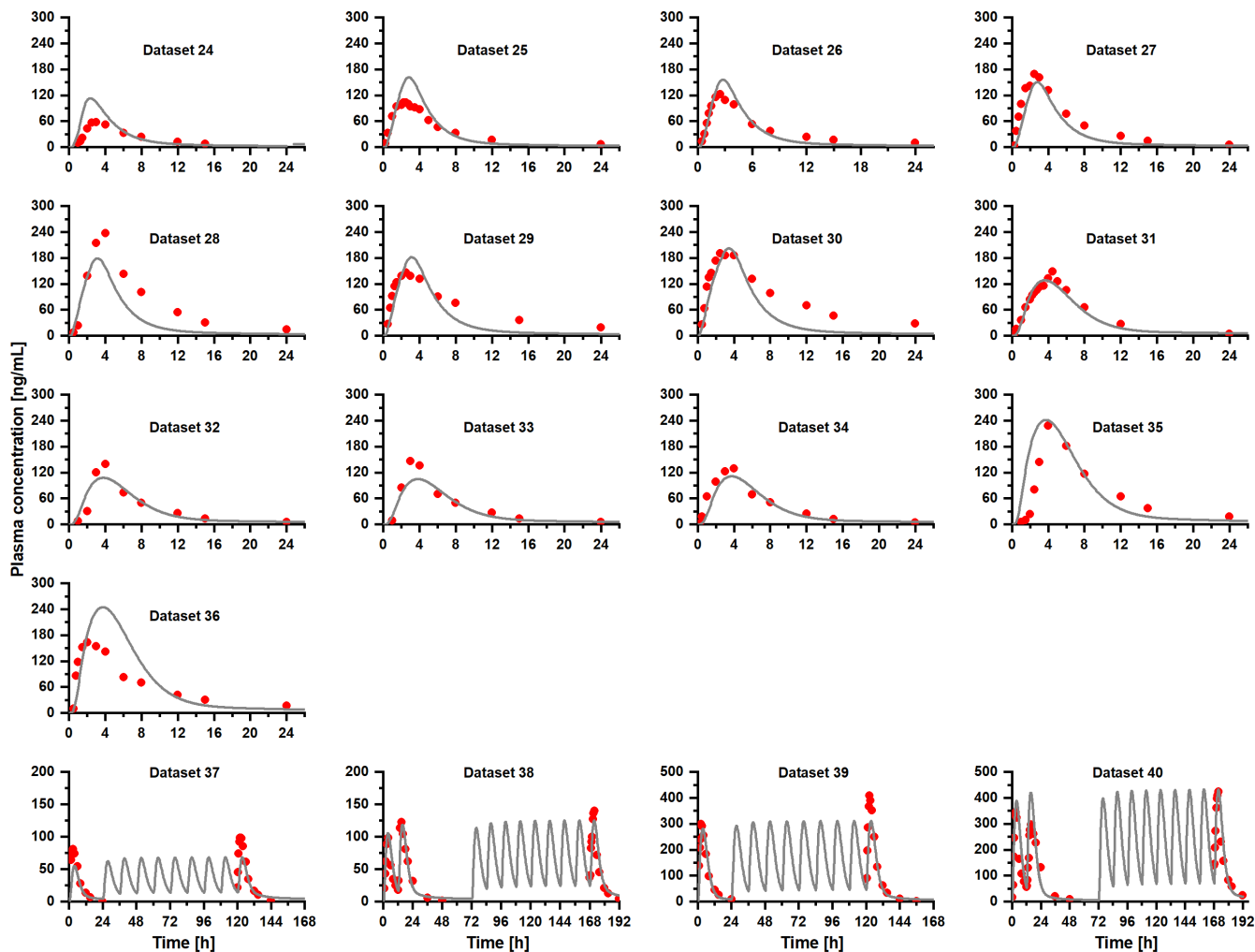


FIGURE 3 Predicted and observed plasma concentration–time curves of RIV after oral administration of RIV in healthy subjects. Test dataset. Solid lines are predicted values of each model. Circles are clinical observations. Details on dosing regimens, characteristics, subject demographics, and references are listed in Table S1. RIV, rivaroxaban.

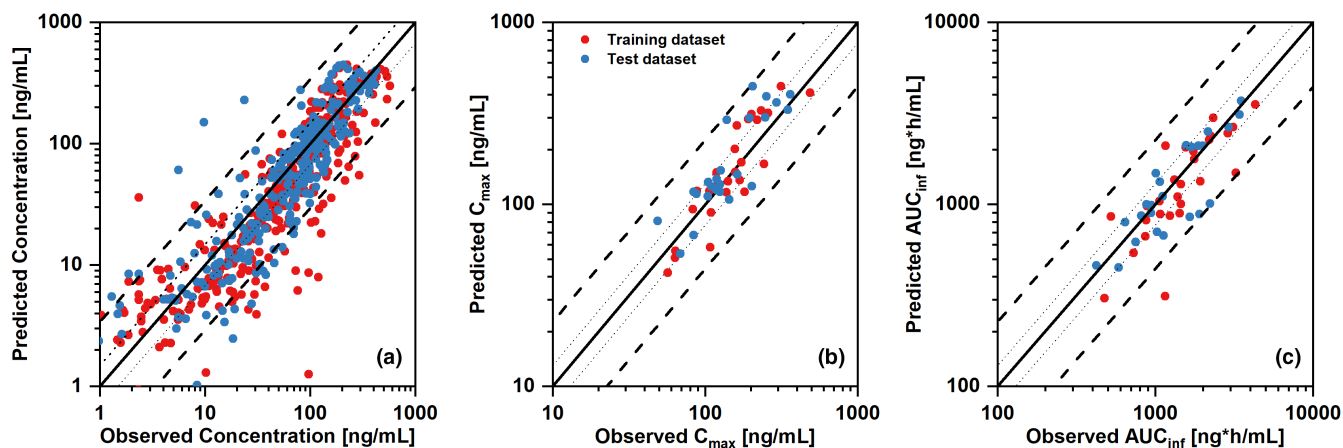


FIGURE 4 Goodness-of-fit plots for the developed PBPK model of RIV for the prediction of (a) plasma concentration, (b) C_{max} , and (c) AUC_{inf} . The line of identity is presented as a solid line; 1.25-fold dimensions and 2.0-fold dimensions are shown using dotted lines and dashed lines, respectively. AUC_{inf} , area under the concentration–time curve from zero to infinity; C_{max} , maximum plasma concentration; PBPK, physiologically-based pharmacokinetic; RIV, rivaroxaban.

of all predicted plasma concentrations fall within two-fold dimensions of the corresponding observed concentrations. The overall MRD value for predicted plasma concentrations of the PBPK model is 1.927. This model is appropriate to be applied for the prediction of DDIs between RIV and CBZ.

Prediction of DDIs between CBZ and RIV

The effects of CBZ on the PKs of RIV were determined by comparing RIV PK profiles when the drug was administered alone and those when the drug was co-administered with CBZ at the steady-state of CBZ. The corresponding RIV plasma concentration-time curve and PK parameters after the first dose and at the steady-state of RIV are illustrated in Table 2 and Figure 5. As seen, CBZ significantly reduced the RIV exposure. Decreases of 35.2% (from 2221.3 to 1438.7 ng*h/ml) and by 25.5% (from 2467.3 to 1838.4 ng*h/ml) in AUC_{inf} and of 37.7% (from 266.3 to 166.1 ng/ml) and 36.4% (from 282.3 to 179.5 ng/ml) in C_{max} were observed at the first dose and at the steady-state of RIV, respectively.

DISCUSSION

DDI is one of the most common causes of adverse drug reactions due to a reduction in the efficacy and/or safety of certain drug(s) that could be a significant cause of post-marketing drug withdrawals.³² Commonly, clinical trial studies were conducted to investigate DDIs; however, due to the high expense, time consumption, and unknown potential risks related, alternative approaches to studying DDIs are imperative. Over the last decade, PK model-based prediction using in vitro and in vivo data has increased significantly.^{33–35}

A PBPK model for RIV was previously developed in adults by Willmann et al.^{8–11} Wherein, the role of the efflux transporter (P-gp) was considered only in the renal elimination process of RIV. The authors assumed that P-gp was the major transport protein accounting for the net tubular secretion of RIV. To scale the developed PBPK model of RIV in adults to pediatrics, the age-dependence of the net tubular secretion was calculated indirectly via the age-dependence of the P-gp transporter in the kidneys of humans.⁸ To predict the RIV potential DDI with P-gp perpetrators, the PK profile of RIV was simulated in

TABLE 2 Predicted PK parameters of RIV following oral administration of RIV 20 mg/day alone or concomitantly with CBZ 900 mg/day simulated by the developed PBPK and PopPK model

Parameters		Unit	RIV alone	RIV + CBZ	Relative change (%)
PBPK model-based approach	AUC_{first}	ng*h/ml	2221.3 (488.3–4087.9)	1438.7 (338.8–3002.0)	35.2
	AUC_{SS}	ng*h/ml	2467.3 (544.6–4667.7)	1838.4 (463.8–3684.4)	25.5
	C_{max_first}	ng/ml	266.3 (80.7–452.3)	166.1 (54.1–299.4)	37.7
	C_{max_SS}	ng/ml	282.3 (86.2–473.6)	179.5 (59.0–321.5)	36.4
	$T_{1/2}$	h	12.9	15.5	–

Note: The subscription of “first” and “SS” stands for “the first dose” and “the steady-state condition”, respectively.

Data are presented as mean (5th percentile–95th percentile), except $t_{1/2}$.

$$\text{Relative change (\%)} = \left[1 - \frac{\text{PK Parameter}_{\text{RIV with CBZ}}}{\text{PK Parameter}_{\text{RIV alone}}} \right] \times 100 (\%).$$

Abbreviations: AUC, area under the concentration-time curve; CBZ, carbamazepine; C_{max} , maximum plasma concentration; PBPK, physiologically-based pharmacokinetic; PK, pharmacokinetic; PopPK, population pharmacokinetic; RIV, rivaroxaban; $T_{1/2}$: elimination half-life.

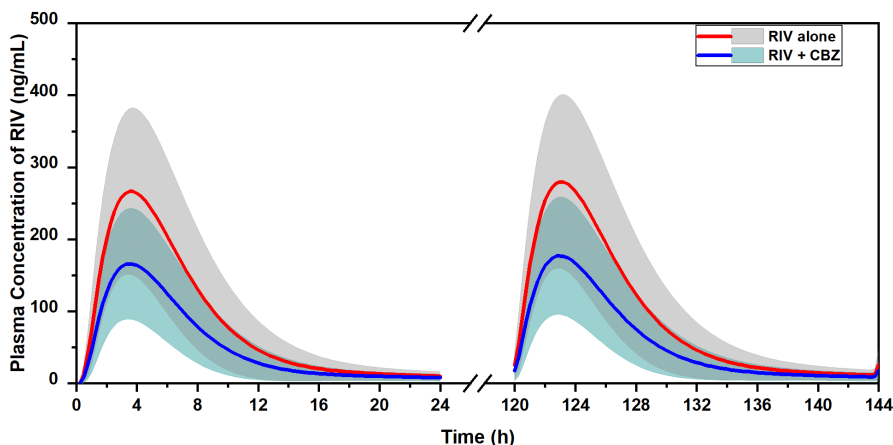


FIGURE 5 Simulated plasma concentration–time profiles of RIV in humans after oral administration at a dose of 20 mg/day with or without the co-administration of CBZ at a dose of 900 mg/day. CBZ, carbamazepine; RIV, rivaroxaban.

individuals with the same biometrics, anatomy, and physiology parameters, but different in P-gp activity, compared to the individuals administered RIV alone. P-gp inhibition of the perpetrators was arbitrarily classified into four categories: no inhibition (0% to <25%), weak inhibition (25% to <50%), weak to moderate inhibition (50% to <75%), and strong inhibition (75% to <100%).¹⁰ Because the authors considered only the efflux function of P-gp in the kidneys, the efflux transport function of P-gp in all other organs, particularly in the gastrointestinal tract and the liver where the P-gp function significantly contributes to the PK of drugs, was not considered. In addition, by just classifying the P-gp inhibition of a perpetrator into one of the four categories, the DDI profiles between RIV and one perpetrator were assumed to be the same even in the different perpetrator dosage scenarios. Of note, the inhibition/induction effects of many drugs are concentration-dependent. To overcome the limitations of the previously developed model of RIV, this study was performed to develop a PBPK model for RIV that includes all the major enzymatic (CYP3A4/2J2 and non-CYP) reactions and transporter (P-gp/BCRP)-mediated transfers. This model considered the active transfer function of these transporters in all expressed locations. When pairing to PBPK models of interest enzyme/transporter perpetrators, the DDI profile of RIV with these perpetrators could be simulated at different dosage scenarios.

Of note, the rate and extent of the drug absorption in the gut are primarily governed by the solubility and the penetration across the gastrointestinal tract of the drug. As RIV is practically insoluble in water (its solubility ranges from 5–25 mg/L), the drug has a solubility-limited absorption profile. However, when RIV is in the solution form, the impact of solubility on the absorption becomes negligible, and intestinal penetration (including the passive intestinal permeability and the P-gp/BCRP efflux mediated transfer) becomes the key factor governing the drug absorption. In this case, the plasma concentration-time profiles of RIV after the oral administration of RIV solutions add significant value to the estimation of the gastrointestinal penetration of RIV. Three plasma concentration-time profiles^{12,21} following oral administration of RIV solutions at the doses of 5 mg and 10 mg were gathered for the initial model development. One available excretion profile in the feces of a patient on RIV after the administration of a 10 mg RIV solution was also used considering that the drug will be eliminated into feces if it did not pass through the gut. In addition, it has been well known that P-gp/BCRP is primarily expressed in the liver and kidneys and contributes to the drug hepatic metabolism and renal elimination. The available hepatic metabolism and renal elimination profiles of RIV after the oral administration of RIV solution also add value to the estimation of both

the hepatic enzymatic reactions and the P-gp/BCRP efflux mediated transfers. In summary, three clinical plasma concentration-time profiles, one fecal elimination profile, one renal elimination profile, and three hepatic enzymatic metabolism profiles were initially used for the estimation of model structure parameters of the PBPK model, especially for the estimation of intestinal permeability, enzymatic reactions, and P-gp/BCRP efflux mediated transfers. These initial PBPK model parameters were then refined by fitting the model to all the training datasets. To inform the optimization of metabolic and transportation kinetics, the DDI between RIV and clarithromycin (a strong CYP3A4 and weak P-gp inhibitor) and the DDI between RIV and fluconazole (a moderate CYP3A4 inhibitor) were added to the training dataset.⁴

It has been determined that food significantly affects the PK of RIV.^{28,36} After a single oral dose of 20 mg of RIV under the fed state, the mean plasma AUC_{inf} and C_{max} increased by 39% (from 1477 to 2048 $\mu\text{g} \times \text{h/L}$) and 76% (from 159.9 to 281.4 $\mu\text{g/L}$), respectively, and the time to reach C_{max} of RIV was prolonged from 2.5 to 4 h compared to the fasted state. PBPK models for RIV, therefore, were developed separately in the fed and fasted states. Our results showed that the enhanced solubility (16.8 vs. 9.9 mg/L) and intestinal permeability ($2.66\text{E-}7$ vs. $3.44\text{E-}7$ cm/s) of RIV accounted for the increased RIV exposure. The prolonged dissolution time (256 vs. 54 min) accounted for the prolonged time to reach C_{max} under the fed state. Relevant ADME processes were predominantly parameterized using literature values.

A case study of CBZ was selected in this study because there was a high possibility of comedication of CBZ with RIV. One of the indications of RIV is the prevention of the risks of stroke and systemic embolism in adults with nonvalvular atrial fibrillation (AF). Whereas, cerebrovascular diseases (disorders in the blood flow to the brain) cause ~40% of epileptic seizures occurring in the elderly, and stroke is the most common type of cerebrovascular event.^{37,38} In patients with stroke-associated seizures, in addition to taking medication long-term for the prevention of stroke, most require chronic treatment with anti-epileptic therapy. To control seizures and epilepsy, CBZ is one of the recommended first-line options.^{39,40} In the literature, adverse events following co-administration of CBZ and RIV have been reported in several case studies.^{41,42} For instance, Stöllberger and Finsterer⁴² reported that venous thrombosis recurred in a 55-year-old male patient who was treated with RIV (20 mg/day) for 4 months (for unprovoked venous thrombosis) and CBZ (900 mg/day) for years (for epilepsy). However, the venous thrombosis was controlled after 5 days when therapy with RIV was stopped and switched to low-molecular-weight

heparin followed by phenprocoumon. The authors suggested that the patient's recurrence of venous thrombosis resulted from insufficient anticoagulation due to a DDI between CBZ and RIV. However, up to date, no studies have investigated the PK DDIs between CBZ and RIV in humans, although DDIs between the two drugs could be expected. As it was reported that a 50% decrease in mean AUC_{inf} of RIV parallelly yields a decrease in its pharmacodynamics.¹ In this case study, the AUC_{inf} of RIV was reduced by 35.2% (from 2221.3 to 1438.7 ng*h/ml) and by 25.5% (from 2467.3 to 1838.4 ng*h/ml) after the first dose and at the steady-state, respectively, whereas the C_{max} of RIV was reduced by 37.7% (from 266.3 to 166.1 ng/ml) and 36.4% (from 282.3 to 179.5 ng/ml), respectively, even when the P-gp transporter-mediated induction effect was not considered to the DDI profile. We suggest that clinical studies should be conducted in humans to obtain a full understanding of their safety and effects when concomitantly administering these drugs.

The present study has some limitations. First of all, this is a common limitation of any PBPK model that they are so complex with many physiological- and drug-dependent parameters. Some parameters can be fixed to data collected in vitro or in vivo, and some are optimized because the related information is unavailable. Therefore, the predicted PK profiles of the drug could be affected significantly by the initial input values of these parameters. In this study, a few parameters were optimized, including specific intestinal permeability; organ permeability, dissolution time, dissolution shape of the RIV tablet; and K_{cat} values for transportation and metabolism processes. The dissolution time and dissolution shape were optimized to describe the delayed time to reach peak concentration under the fed state. It might come from the reduced interface of the tablet with the intestinal wall due to the presence of food that could not be stimulated in the in vitro experiment. For non-CYP-mediated reactions, CES1, which is located in the liver and responsible for the hydrolysis of ester and amide bonds of many drugs, was introduced into the model as a representative. The K_m value for the non-CYP-mediated reaction was assumed as the same as that of the CYP3A4 reaction. In addition, the K_{cat} values for both enzymatic reactions and transporter-mediated transfer were optimized due to the lack of in vitro and in vivo data. Results from the sensitivity analysis (Supplementary Material S1) showed that the initial input parameters do not significantly impact the prediction of the PK profile of RIV. Both K_m and K_{cat} values are not part of the parameters accounting for the most sensitive of the PKs of RIV. The fraction unbound in plasma and the specific intestinal permeability are the two most sensitive factors and their sensitivity is not significant. A 10%

increase in the fraction unbound leads to a 9.5% decrease in the AUC value. A 10% increase in the specific intestinal permeability leads to a 9.4% increase in the AUC value of RIV. Therefore, our strategy of model development does not significantly impact the PK profile of RIV. Second, there is another common limitation of a PBPK model-based approach. In the case of a DDI study, it would be impossible to predict the full impact of concomitant drug administration if the enzymes/transporters involved in their metabolism are not known. In the present study, a PBPK model for RIV, that included all the major enzyme reactions and transporter-mediated transportation, has been well developed. However, when pairing to an adopted PBPK model of CBZ (that was previously developed by Fuhr et al.³¹) to predict the DDI profile between them, the P-gp transporter-mediated induction effect of CBZ was not counted in the DDI simulation. The reason was that the induction effect of CBZ on the P-gp transporter was not implemented in the developed CBZ model due to a lack of in vitro and in vivo experiments concerning the reaction. However, this is not a limitation of the RIV PBPK model itself, this model could show good performance in the prediction of DDI profiles of RIV with other interested CYP3A4/P-gp perpetrators by pairing to their PBPK models.

AUTHOR CONTRIBUTIONS

L.T.N., S.-Y.Y., and J.-W.C. wrote the manuscript. L.T.N., S.-Y.Y., S.Y.S., D.T.C., H.V.N., S.K.J., J.-Y.L., J.-H.L., H.Y.Y., and J.-W.C. designed the research. L.T.N., S.-Y.Y., H.-Y.Y., and J.-W.C. performed the research. L.T.N., S.-Y.Y., and J.-W.C. analyzed the data.

FUNDING INFORMATION

This study was supported by the Institute of Information & Communications Technology Planning & Evaluation (IITP) grant funded by the Korean government (MSIT; No. 2020-0-01441, Artificial Intelligence Convergence Research Center [Chungnam National University], No. RS-2022-00155857, Artificial Intelligence Convergence Innovation Human Resources Development [Chungnam National University]) and National Research Foundation of Korea (NRF) grant funded by the Korea government (MSIT; No. NRF-2018R1C1B5085278, NRF-2022R1A2C1010929), and the Korea Environmental Industry & Technology Institute (KEITI) through Core Technology Development Project for Environmental Diseases Prevention and Management (2021003310001), funded by the Korea Ministry of Environment (MOE).

CONFLICT OF INTEREST

The authors declared no competing interests in this work.

ORCID

Lien Thi Ngo  <https://orcid.org/0000-0002-0577-4983>
 Sooyoung Shin  <https://orcid.org/0000-0003-2388-1122>
 Duc Tuan Cao  <https://orcid.org/0000-0001-9129-8241>
 Hung Van Nguyen  <https://orcid.org/0000-0002-6830-5279>
 Hwi-yeol Yun  <https://orcid.org/0000-0001-8793-2449>
 Jung-woo Chae  <https://orcid.org/0000-0001-6026-7063>

REFERENCES

1. Bayer Pharma AG *Xarelto (rivaroxaban) Summary of Product Characteristics*; 2013. https://www.ema.europa.eu/en/documents/product-information/xarelto-epar-product-information_en.pdf
2. European Medicines Agency. *CHMP assessment report for Xarelto*; 2008. https://www.ema.europa.eu/en/documents/assessment-report/xarelto-epar-public-assessment-report_en.pdf
3. Mueck W, Stampfuss J, Kubitzka D, Becka M. Clinical pharmacokinetic and pharmacodynamic profile of rivaroxaban. *Clin Pharmacokinet*. 2014;53:1-16. doi:10.1007/s40262-013-0100-7
4. Mueck W, Kubitzka D, Becka M. Co-administration of rivaroxaban with drugs that share its elimination pathways: pharmacokinetic effects in healthy subjects. *Br J Clin Pharmacol*. 2013;76:455-466.
5. Gnoth MJ, Buetehorn U, Muenster U, Schwarz T, Sandmann S. In vitro and in vivo P-glycoprotein transport characteristics of rivaroxaban. *J Pharmacol Exp Ther*. 2011;338:372-380.
6. Hodin S, Basset T, Jacquereux E, et al. In vitro comparison of the role of P-glycoprotein and breast cancer resistance protein on direct Oral anticoagulants disposition. *Eur J Drug Metab Pharmacokinet*. 2018;43:183-191.
7. Gong IY, Mansell SE, Kim RB. Absence of both MDR1 (ABCB1) and breast cancer resistance protein (ABCG2) transporters significantly alters rivaroxaban disposition and central nervous system entry. *Basic Clin Pharmacol Toxicol*. 2013;112:164-170.
8. Willmann S, Becker C, Burghaus R, et al. Development of a Paediatric population-based model of the pharmacokinetics of rivaroxaban. *Clin Pharmacokinet*. 2014;53:89-102.
9. Ince I, Dallmann A, Frechen S, et al. Predictive performance of physiology-based pharmacokinetic dose estimates for pediatric trials: evaluation with 10 Bayer small-molecule compounds in children. *J Clin Pharmacol*. 2021;61:S70-S82.
10. Willmann S, Coboeken K, Kapsa S, et al. Applications of physiologically based pharmacokinetic modeling of rivaroxaban—renal and hepatic impairment and drug-drug interaction potential. *J Clin Pharmacol*. 2021;61:656-665.
11. Willmann S, Thelen K, Kubitzka D, et al. Pharmacokinetics of rivaroxaban in children using physiologically based and population pharmacokinetic modelling: an EINSTEIN-Jr phase I study. *Thromb J*. 2018;16:32.
12. Kubitzka D, Becka M, Voith B, Zuehlsdorf M, Wensing G. Safety, pharmacodynamics, and pharmacokinetics of single doses of BAY 59-7939, an oral, direct factor Xa inhibitor. *Clin Pharmacol Ther*. 2005;78:412-421.
13. Johannessen SI, Landmark CJ. Antiepileptic drug interactions – principles and clinical implications. *Curr Neuropharmacol*. 2010;8:254-267.
14. Patsalos PN, Fröscher W, Pisani F, Rijn CM. The importance of drug interactions in epilepsy therapy. *Epilepsia*. 2002;43:365-385.
15. Owen A, Goldring C, Morgan P, Park BK, Pirmohamed M. Induction of P-glycoprotein in lymphocytes by carbamazepine and rifampicin: the role of nuclear hormone response elements. *Br J Clin Pharmacol*. 2006;62:237-242.
16. Giessmann T, May K, Modess C, et al. Carbamazepine regulates intestinal P-glycoprotein and multidrug resistance protein MRP2 and influences disposition of talinolol in humans. *Clin Pharmacol Ther*. 2004;76:192-200.
17. Vlase L, Popa A, Neag M, Muntean D, Bâldea I, Leucuta SE. Pharmacokinetic interaction between zolpidem and carbamazepine in healthy volunteers. *J Clin Pharmacol*. 2011;51:1233-1236.
18. Yamada S, Yasui-Furukori N, Akamine Y, Kaneko S, Uno T. Effects of the P-glycoprotein inducer carbamazepine on fexofenadine pharmacokinetics. *Ther Drug Monit*. 2009;31:764-768.
19. Vlase L, Neag M, Popa A, Muntean D, Bâldea I, Leucuta SE. Pharmacokinetic interaction between ivabradine and carbamazepine in healthy volunteers. *J Clin Pharm Ther*. 2011;36:225-229.
20. WebPlotDigitizer. <https://automeris.io/WebPlotDigitizer/>
21. Weinz C, Schwarz T, Kubitzka D, Mueck W, Lang D. Metabolism and excretion of rivaroxaban, an Oral, direct factor Xa inhibitor, in rats, dogs, and humans. *Drug Metab Dispos*. 2009;37:1056-1064.
22. U.S. Food and Drug Administration XARELTO® (rivaroxaban): Prescribing Information; 2011.
23. Samama MM. The mechanism of action of rivaroxaban – an oral, direct factor Xa inhibitor – compared with other anticoagulants. *Thromb Res*. 2011;127:497-504.
24. Drugbank. Drugbank-Rivaroxaban. <https://go.drugbank.com/drugs/DB06228>
25. Remko M. Molecular structure, lipophilicity, solubility, absorption, and polar surface area of novel anticoagulant agents. *J Mol Struct THEOCHEM*. 2009;916(1-3):76-85. doi:10.1016/j.theochem.2009.09.011
26. Weinz C, Buetehorn U, Daehler H-P, et al. Pharmacokinetics of BAY 59-7939 – an oral, direct factor Xa inhibitor – in rats and dogs. *Xenobiotica*. 2005;35(9):891-910. doi:10.1080/00498250500250493
27. Chen ML, Yu L, Grillo JA, et al. Safety, pharmacokinetics and pharmacodynamics of single/multiple doses of the oral, direct factor Xa inhibitor rivaroxaban in healthy Chinese subjects. *Br J Clin Pharmacol*. 2009;68(1):77-88. doi:10.1111/j.1365-2125.2009.03390.x
28. Kushwah V, Arora S, Tamás Katona M, Modhave D, Fröhlich E, Paudel A. On absorption modeling and food effect prediction of rivaroxaban, a BCS II drug orally administered as an immediate-release tablet. *Pharmaceutics*. 2021;13:283.
29. Takács-Novák K, Szőke V, Völgyi G, Horváth P, Ambrus R, Szabó-Révész P. Biorelevant solubility of poorly soluble drugs: rivaroxaban, furosemide, papaverine and niflumic acid. *J Pharm Biomed Anal*. 2013;83:279-285. doi:10.1016/j.jpba.2013.05.011
30. Zhao T, Chen Y, Wang D, et al. Identifying the dominant contribution of human cytochrome P450 2J2 to the metabolism of rivaroxaban, an Oral anticoagulant. *Cardiovasc Drugs Ther*. 2021;36:121-129. doi:10.1007/s10557-020-07129-z
31. Fuhr LM, Marok FZ, Hanke N, Selzer D, Lehr T. Pharmacokinetics of the CYP3A4 and CYP2B6 inducer carbamazepine and its drug-drug interaction potential: a

- physiologically based pharmacokinetic modeling approach. *Pharmaceutics*. 2021;13:270.
32. Onakpoya IJ, Heneghan CJ, Aronson JK. Post-marketing withdrawal of anti-obesity medicinal products because of adverse drug reactions: a systematic review. *BMC Med*. 2016;14:191.
 33. Emoto C, McPhail BT, Fukuda T. Clinical applications of physiologically based pharmacokinetic modeling: perspectives on the advantages and challenges. *Ther Drug Monit*. 2020;42:157-158.
 34. Einolf HJ. Comparison of different approaches to predict metabolic drug-drug interactions. *Xenobiotica*. 2007;37:1257-1294.
 35. Yeo KR, Jamei M, Rostami-Hodjegan A. Predicting drug-drug interactions: application of physiologically based pharmacokinetic models under a systems biology approach. *Expert Rev Clin Pharmacol*. 2013;6:143-157.
 36. Stampfuss J, Kubitzka D, Becka M, Mueck W. The effect of food on the absorption and pharmacokinetics of rivaroxaban. *Int J Clin Pharmacol Ther*. 2013;51:549-561.
 37. Myint PK, Staufenberg EFA, Sabanathan K. Post-stroke seizure and post-stroke epilepsy. *Postgrad Med J*. 2006;82:568-572.
 38. Lühdorf K, Jensen LK, Plesner AM. Etiology of seizures in the elderly. *Epilepsia*. 1986;27:458-463.
 39. Reuck JL. Management of stroke-related seizures. *Acta Neurol Belg*. 2009;109:271-276.
 40. Ferro JM, Pinto F. Poststroke epilepsy: epidemiology, pathophysiology and management. *Drugs Aging*. 2004;21:639-653.
 41. Risselada AJ, Visser MJ, van Roon EN. Pulmonary embolism due to interaction between rivaroxaban and carbamazepine. *Ned Tijdschr Geneesk*. 2013;157:A6568.
 42. Stöllberger C, Finsterer J. Recurrent venous thrombosis under rivaroxaban and carbamazepine for symptomatic epilepsy. *Neurol Neurochir Pol*. 2017;51:194-196.

SUPPORTING INFORMATION

Additional supporting information can be found online in the Supporting Information section at the end of this article.

How to cite this article: Ngo LT, Yang S-y, Shin S, et al. Application of physiologically-based pharmacokinetic model approach to predict pharmacokinetics and drug-drug interaction of rivaroxaban: A case study of rivaroxaban and carbamazepine. *CPT Pharmacometrics Syst Pharmacol*. 2022;11:1430-1442. doi:[10.1002/psp4.12844](https://doi.org/10.1002/psp4.12844)